physchem

MDPI

Article

Molecular Structure and Medium Effects on Porphyrin Photostability in Aqueous Solutions

Lubov Vasileva [1], Anastasia Povolotckaia [2], Elizaveta Chebanova [1], Daniil Lukyanov [1] and Alexey Povolotskiy [1,*]

[1] Institute of Chemistry, Saint-Petersburg State University, 198504 St. Petersburg, Russia; lubovvasileva85472@gmail.com (L.V.); st117566@student.spbu.ru (E.C.); d.lukianov@spbu.ru (D.L.)
[2] Center for Optical and Laser Materials Research, Saint-Petersburg State University, 198504 St. Petersburg, Russia; anastasia.povolotckaia@spbu.ru
* Correspondence: alexey.povolotskiy@spbu.ru

Abstract

The photostability of tetraphenylporphyrin, zinc(II) tetraphenylporphyrin, and 5,10,15,20-tetrakis(1-methylpyridinium-4-yl)porphyrin p-toluenesulfonate was quantified in water and DMSO/water mixtures by absorption and 650-nm photoluminescence under 423-nm excitation. Under air in DMSO/water, the apparent degradation rate constants increased in the order TPP (0.033 min^{-1}) < ZnTPP (0.046 min^{-1}) < TMPyP–OTs (0.139 min^{-1}); thus, TMPyP–OTs degraded about 4.2 times faster than TPP. Argon deaeration reduced the rate constants to 0.013, 0.028, and 0.034 min^{-1}, respectively, confirming the dominant contribution of oxygen-dependent pathways in air; the largest stabilization was observed for TMPyP–OTs (4.1-fold). DMSO/water accelerated the degradation of TMPyP–OTs 5.3-fold under air but only 1.6-fold after deaeration, linking the solvent effect to singlet-oxygen-mediated processes. In deaerated water, increasing the temperature from 25 to 45 °C increased the rate constant from 0.019 to 0.048 min^{-1} (2.5-fold), revealing a significant oxygen-independent contribution. These data indicate that steric meso-shielding, metalation, peripheral substituents, aggregation propensity, oxygen, solvent, and temperature jointly control porphyrin photostability. The quantitative ranking provides selection criteria for porphyrin luminophores in hybrid nanomaterials: TPP-like scaffolds are preferable when high photostability is required, whereas the higher reactivity of TMPyP–OTs is advantageous for photodynamic therapy provided that oxygen and solvent conditions are carefully controlled.

Keywords: porphyrins; photostability; photodegradation; singlet oxygen; photoluminescence; dimethyl sulfoxide

Check for updates

Academic Editors: Eralci Moreira Therézio and Paulo Ernesto Marchezi

Received: 15 October 2026
Revised: 6 November 2026
Accepted: 10 November 2026
Published: 13 November 2026

Copyright: © 2026 by the authors. Licensee MDPI, Basel, Switzerland. This article is an open access article distributed under the terms and conditions of the Creative Commons Attribution (CC BY) license.

1. Introduction

Porphyrins are a broad class of macrocyclic compounds whose planar aromatic system consists of four pyrrole rings connected by methine bridges. This structure forms a conjugated π-system and determines visible-light absorption, luminescence, and complexation [1–7]. The parent compound, porphin, can be modified at the β-pyrrolic and meso positions. Natural porphyrins such as heme and chlorophyll contain alkyl, vinyl, and carboxyl groups, whereas synthetic meso-substitution is widely used because it preserves aromaticity and allows directed functionalization [1,2]. Tetraphenylporphyrin (TPP), with four meso-phenyl rings, is a key synthetic platform [3,4]. Electron-donating substituents, for example, amino groups in NH_2TPP and $(NH_2)_4$TPP, increase electron density, stabilize the HOMO, lower the optical transition energy, cause a bathochromic shift, and alter redox

potentials [2,6,7]. Porphyrins also act as ligands: four inwardly directed pyrrole nitrogen atoms bind metal cations to form metalloporphyrins with properties different from those of nonmetallated forms [3,5].

The stability and optical properties of porphyrins are governed by electronic structure and geometry [6–9]. When the π-electron count follows Hückel's rule [4n + 2], the macrocycle is highly stable and shows clear absorption and fluorescence, nanosecond excited-state lifetimes, and strong two-photon absorption [3,4,6]. A planar, rigid structure ensures π-electron delocalization; twisting or flexibility disrupts conjugation, increases nonradiative losses, and reduces photostability [7,10]. Neutral porphyrins typically display four Q bands and an intense Soret band near 400 nm, reflecting D_2h symmetry [3,4,6]. Metalation or protonation raises symmetry to D_4h and simplifies the spectrum to two bands [1–7]. Hydrogenation, aza-substitution, conjugation extension, and aggregation also affect absorption [6–8]. Aggregation is especially relevant to hybrid nanoparticles, where new broad bands or shifts indicate intermolecular interactions [8,11–14].

Luminescence properties, including fluorescence quantum yield (φ) and excited-state lifetime (τ), follow from electronic structure [6,15]. The aromatic π-system provides red and near-infrared emission (600–800 nm) from the $S_1 \rightarrow S_0$ transition [6,16]. Electron-donating meso substituents increase φ, whereas electron-withdrawing groups such as $–NO_2$ and –CHO open nonradiative channels and quench fluorescence [6,7,15]. Diamagnetic Zn^{2+} complexes generally remain fluorescent, while paramagnetic Mn^{2+}, Cu^{2+}, and Co^{2+} efficiently quench emission through spin–orbit coupling and charge transfer [8,10]. Plasmonic nanostructures can enhance emission via metal-enhanced fluorescence (MEF), requiring spectral overlap and a dielectric spacer [5]. Aggregated fractions are often nonfluorescent and photochemically inactive, complicating effective quantum yield prediction [8,11–14].

These properties make porphyrins valuable in photomedicine, bioimaging, sensing, artificial photosynthesis, and optoelectronics [11,16–18]. In hybrid molecular–plasmonic nanomaterials, metal nanoparticles act as optical heaters, while surface porphyrins serve as luminescent thermometers and sensors. Such systems are relevant to photothermal therapy (PTT), where local temperature control is critical [5]. Porphyrins also generate singlet oxygen and serve as photosensitizers in photodynamic therapy (PDT) [15,17,18]. Practical performance depends on photostability. Photodegradation involves irreversible light-initiated transformations. In aerobic media, the oxygen-dependent pathway dominates: triplet porphyrin transfers energy to oxygen, producing singlet oxygen, which attacks the macrocycle [10,15,19–28]. In deaerated media, oxygen-independent pathways dominate, including electron transfer from solvent, radical-anion formation, protonation, and macrocycle opening [7,9,10]. Structure, metalation, substituents, aggregation, solvent, oxygen, and temperature all influence these pathways [25–29].

Therefore, this work aims to determine the influence of porphyrin molecular structure and environmental parameters on the photodissociation rate [1–15,18,19,29]. It analyzes the literature on porphyrin-based hybrid nanoparticles, measures photodegradation kinetics by spectrophotometry and spectrofluorimetry, determines rate constants for different structures and conditions, and identifies the most photostable porphyrins [27–29]. Such data are essential for predicting the performance of porphyrin-based luminophores in hybrid nanomaterials and for selecting optimal compounds for photomedicine and bioimaging [25–29].

2. Materials and Methods

2.1. Reagents

All reagents were of analytical or spectroscopic grade and were used as received unless otherwise stated. Deionized water (H_2O, CAS 7732-18-5, resistivity 18.2 MΩ·cm at 25 °C, Simplicity UV, Merck Millipore, Darmstadt, Germany) and dimethyl sulfoxide (DMSO,

C_2H_6OS, MW 78.13, CAS 67-68-5, ≥99.9%, spectroscopic grade, Sigma-Aldrich, Darmstadt, Germany) were used as solvents. Argon (Ar, CAS 7440-37-1, purity ≥ 99.99%, Nord Gaz, St. Petersburg, Russia) was used for deaeration of solutions.

The structures of the porphyrins used in this work as model systems for photodegradation studies are presented in Figure 1. The following porphyrins were used: 5,10,15,20-tetraphenyl-21H,23H-porphine (TPP, $C_{44}H_{30}N_4$, MW 614.75, CAS 917-23-7, purity ≥ 95%); zinc(II) 5,10,15,20-tetraphenyl-21H,23H-porphine (ZnTPP, $C_{44}H_{28}N_4Zn$, MW 678.12, CAS 14074-80-7, purity ≥ 95%); and 5,10,15,20-tetrakis(1-methylpyridinium-4-yl)-21H,23H-porphine tetrakis(p-toluenesulfonate) (TMPyP–OTs, $C_{72}H_{66}N_8S_4O_{12}$, MW 1363.62, CAS 62516-18-3, purity ≥ 95%). The porphyrins were synthesized at the Institute of Chemistry, St. Petersburg State University (St. Petersburg, Russia), and were used without further purification. Their identity and purity were confirmed by UV-Vis absorption spectroscopy in the corresponding solvents before kinetic experiments.

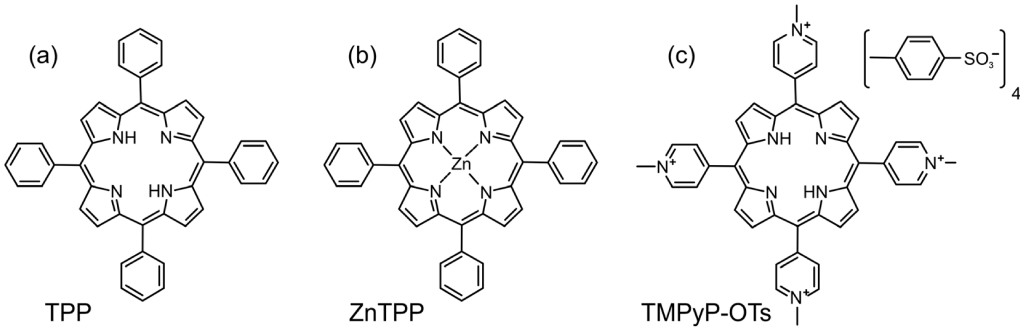


Figure 1. Structures of the porphyrins: (**a**) 5,10,15,20-tetraphenyl-21H,23H-porphine; (**b**) zinc(II) 5,10,15,20-tetraphenyl-21H,23H-porphine; (**c**) 5,10,15,20-tetrakis(1-methylpyridinium-4-yl)-21H,23H-porphine tetrakis(p-toluenesulfonate).

Stock solutions of porphyrins were prepared in DMSO or water, protected from light, and stored at 4 °C until use. DMSO was chosen as a polar aprotic solvent for preliminary dissolution of water-insoluble porphyrins. Deionized water was used for aqueous solutions and for DMSO/water mixtures. Argon was of high purity and was used to remove dissolved oxygen from solutions prior to and during oxygen-independent photodegradation measurements.

2.2. Sample Preparation

The initial concentrations of the solutions were selected so that the optical density in the Soret band region was approximately 0.1 (C(TPP) = 0.22 μM, C(ZnTPP) = 0.17 μM, C(TMPyP-OTs) = 0.45 μM). Measurements were performed in a cuvette with an optical path length of 1 cm. Absorption spectra were recorded in the range 300–700 nm. For water-insoluble porphyrins, small amounts of DMSO were used for preliminary dissolution. To ensure comparable conditions, water-soluble TMPyP–OTs was also measured with proportional DMSO addition. For oxygen-independent measurements, solutions were bubbled with argon for 10 min and then kept under continuous argon bubbling during kinetic measurements.

2.3. Spectroscopic Measurements

Absorption spectra were recorded on a two-beam UV-3600 spectrophotometer (Shimadzu, Kyoto, Japan) equipped with a double monochromator and a photomultiplier detector. Quartz cuvettes with an optical path length of 1 cm were used. Spectra were acquired in the wavelength range 300–700 nm with a spectral resolution of 1 nm, a scan speed of 200 nm min^{-1}, and a data interval of 0.5 nm. Baseline correction was performed using the corresponding pure solvent (water, DMSO, or DMSO/water mixture) in the

reference channel. All measurements were carried out at room temperature (25 ± 1 °C) unless otherwise stated. The instrument was controlled by UVProbe software Versions 2.33 (Shimadzu). For each sample, at least three independent spectra were recorded and averaged to improve the signal-to-noise ratio.

Luminescence spectra were recorded on a modular Fluorolog-3 spectrofluorimeter (Horiba, Kyoto, Japan) equipped with a 450 W xenon lamp as the excitation source and an R928P photomultiplier tube (Hamamatsu, Japan) as the detector. The instrument operated in the right-angle geometry using quartz cuvettes with a 1 cm path length. Excitation was performed at 423 nm, corresponding to the maximum of the Soret band. Emission spectra were recorded in the range 550–800 nm with a spectral resolution of 1 nm, an integration time of 0.1 s, and a scan speed of 240 nm min^{-1}. The spectra were corrected for the spectral response of the detection system using the correction file provided by the manufacturer. All measurements were performed at room temperature (25 ± 1 °C). The instrument was controlled by FluorEssence software Version v3.8 (Horiba). For each sample, at least three spectra were recorded and averaged.

The absorption and photoluminescence spectra of porphyrins are presented in Figure 2. The blue vertical band corresponds to the pump wavelength of the femtosecond laser, and the red line indicates the emission wavelength at which the luminescence intensity was recorded when measuring the photodegradation kinetic curves of porphyrins.

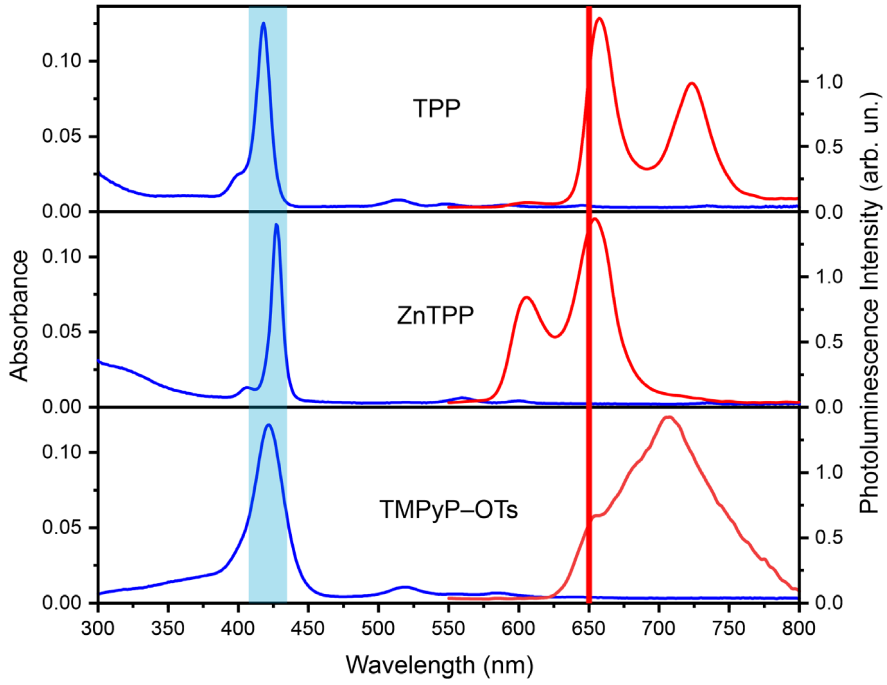


Figure 2. Absorption spectra (blue curves) and photoluminescence spectra upon excitation into the Soret band (red lines) for the porphyrins under study.

2.4. Photodegradation Kinetics

The porphyrin concentration was selected so that the optical density of the solution at the excitation wavelength was approximately 0.1 for a cuvette with an optical path length of 1 cm (Figure 2). At such optical density values, light absorption can be considered linear, which minimizes adverse effects such as the inner filter effect and inhomogeneous intensity of the exciting radiation over the cuvette volume. Since the optical density of the solutions at the excitation wavelength is about 0.1 and the photodegradation kinetic curves

of all samples obey an exponential law, the observed porphyrin photodegradation reactions proceed according to first-order kinetics:

$$C(t) = C_0 \cdot e^{-kt}$$

where $C(t)$ is the porphyrin concentration of the substance at time t, C_0 is the initial concentration, and k is the first-order reaction rate constant. Given the linear regime and the linear relationship between the concentration of excited molecules and the luminescence intensity in accordance with the Einstein coefficients, the rate of change in luminescence intensity strictly corresponds to the rate of change in porphyrin concentration.

The schematic diagram of the experimental setup for measuring the photodegradation rate of porphyrins is presented in Figure 3. The setup is based on a Mira-900D femtosecond laser (Coherent, Santa Clara, CA, USA) as the excitation source. The laser wavelength was tuned to 423 nm (Full Width at Half Maximum (FWHM) = 15 nm), which corresponds to the Soret band absorption maximum of all studied porphyrins. The laser operated at a repetition rate of 76 MHz with a pulse duration of 150 fs and an average power of 220 mW. These conditions provided quasi-continuous excitation, ensuring efficient population of the excited singlet state while avoiding significant heating of the solution. Uniform irradiation of the sample was ensured by placing 1 mL of porphyrin solution in a standard quartz optical cuvette with four polished windows and irradiating the cuvette with a defocused laser beam so that uniform luminescence was observed throughout the entire volume. More uniform irradiation was achieved by continuously stirring the solution in the cuvette using a magnetic stirrer. Argon bubbling was performed before the photodegradation kinetics measurements until oxygen was displaced from the solution and was continued during the recording of the kinetic curves to prevent oxygen from the atmosphere from dissolving in the solution. The time required for preliminary bubbling was determined using the triplet-state lifetime of the porphyrins (from the delayed fluorescence signal), since it is in the triplet state that porphyrins in solution collide with dissolved oxygen and transfer excitation energy, as a result of which triplet oxygen is converted into singlet oxygen. In the presence of oxygen, the lifetime is 1 μs; upon bubbling, the lifetime increases (the relaxation channel via collision with oxygen decreases) and after 10 min stops changing, which indicates the absence of oxygen in the solution. Bubbling was performed through a Drechsel bottle containing the solvent, which kept the solvent level in the cuvette constant during argon bubbling and consequently prevented changes in porphyrin concentration. The influence of temperature during the recording of kinetic curves was excluded by thermostating the cuvette using a water thermostat maintaining the temperature at a specified level with an accuracy of ±0.5 °C. The incident power was measured with a power meter (Coherent, USA) before each experiment and kept constant throughout the measurements.

The luminescence decay kinetics were recorded at 650 nm, corresponding to the maximum of the porphyrin fluorescence band, using an original setup based on a double monochromator MDR-6 (LOMO, St. Petersburg, Russia), a photomultiplier tube (Hamamatsu, Hamamatsu, Japan), and an analog-to-digital converter (National Instruments, Austin, TX, USA). The monochromator slit width was set to 1 nm. The photomultiplier was operated at a voltage of 900 V. The luminescence signal was collected at 90° to the excitation beam. The signal was digitized with a sampling rate of 1 kHz and recorded continuously for 1 h. Before each kinetic measurement, the sample was kept in the dark for 5 min to ensure complete adaptation. For temperature-dependent measurements, the cuvette was placed in a temperature stabilized holder (accuracy ±0.5 °C) and equilibrated at different temperatures in the range of 25–45 °C for 10 min before irradiation. Each kinetic curve was recorded at least three times to ensure reproducibility.

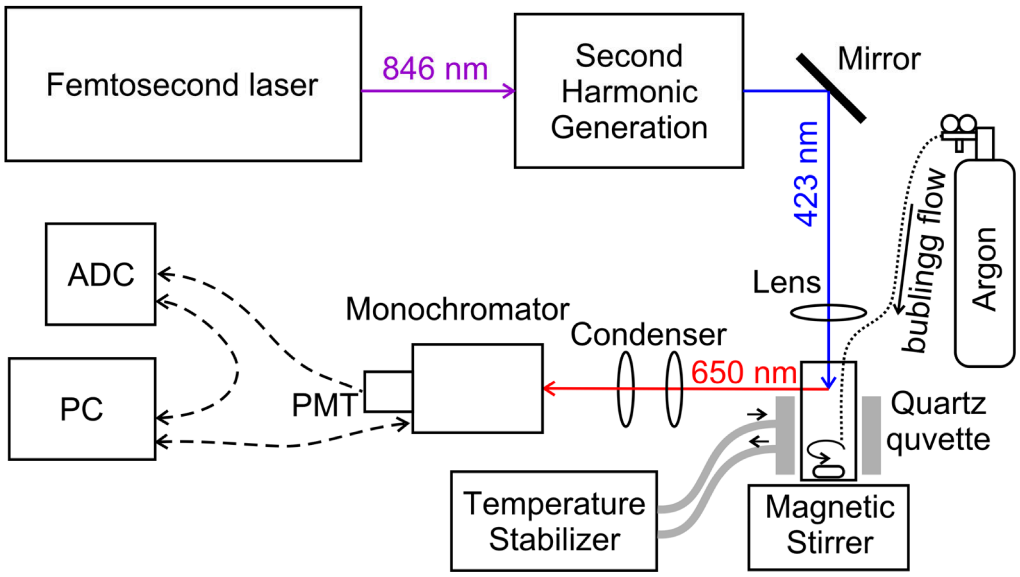


Figure 3. The schematic diagram of the experimental setup for measuring the photodegradation rate of porphyrins. The analog signal of the photomultiplier tube (PMT) was digitized using an analog-to-digital converter (ADC) and recorded on a personal computer (PC).

Confidence intervals were calculated using the Student's coefficient at a confidence probability $p = 0.95$.

2.5. Data Analysis

The absorption of light by porphyrin solutions was described using the Bouguer–Lambert–Beer law, according to which the optical density is directly proportional to the concentration of the absorbing species and the optical path length. This relationship allowed the decrease in absorption at the Soret band maximum to be used as a measure of porphyrin concentration during photodegradation.

Kinetic curves were linearized in coordinates corresponding to the assumed kinetic model. The linearity of these plots confirmed the reaction order, and the slope of the linear approximation was taken as the apparent rate constant of photodissociation, k. It should be emphasized that the rate constants reported here are apparent (effective) constants derived from the decrease in the 650-nm photoluminescence intensity under continuous irradiation. They characterize the overall change in the luminescence response of the system under the given conditions and are not equivalent to intrinsic photodegradation quantum yields. The distinction is important because, as shown by Golec et al. [30], oxygen removal can simultaneously suppress the dominant degradation channel and lengthen the triplet-state lifetime, so that quantum yields and measured rates may change in opposite directions. In the present work, the apparent constants are therefore used for the comparative ranking of photostability under identical conditions, not as absolute measures of photochemical efficiency. The rate constants were determined for each porphyrin under different conditions.

3. Results

The kinetics of porphyrin photodegradation can be measured by both absorption and luminescence methods. The absorption method is based on periodic recording of absorption spectra at different irradiation times. As an example, Figure 4a shows the absorption spectra of a TMPyP–OTs solution after irradiation at 423 nm for various times. From the obtained absorption spectra, the dependence of optical density at the Soret band maximum on irradiation time was plotted (inset graph in Figure 4a). This method has several drawbacks,

the main ones being associated with the need for sequential irradiation of the sample and measurement of absorption spectra, which interrupts magnetic stirring, argon bubbling, and temperature stabilization. All of this often leads to deviations from the exponential shape of the kinetic curve, indicating experimental errors and leading to an error in the determined photodissociation rate constants exceeding 10%. When the rate constant is determined from the fluorescence signal, the error in the measured rate constant does not exceed 7%, and all kinetic curves obey the exponential law. These drawbacks can be avoided by using the photoluminescence intensity rather than absorption as the optical response proportional to the molecular concentration. Because the photoluminescence intensity at 650 nm depends not only on the concentration of the intact porphyrin but also on the excited-state relaxation pathways, part of the observed signal change may have a photophysical origin. Solvent composition and hydrogen-bonding interactions are known to modify the fluorescence behavior of pyridyl-substituted porphyrins [31], and this possibility is therefore considered explicitly in the Discussion section.

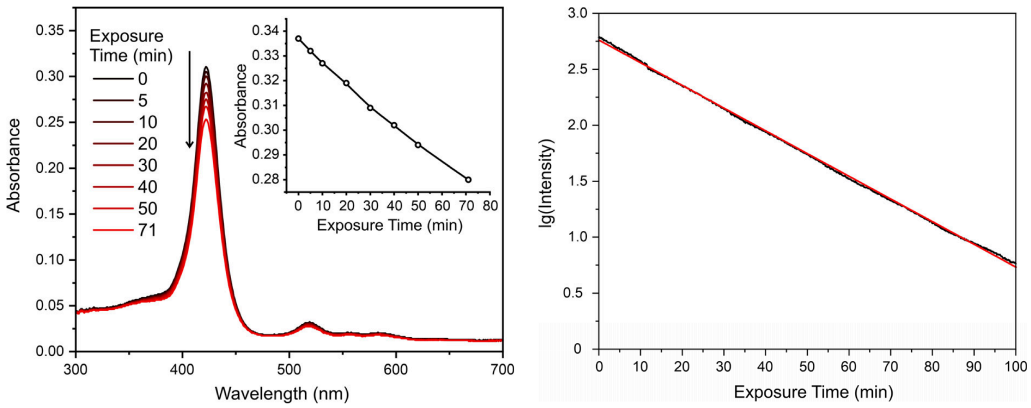


Figure 4. (**a**) Absorption spectra of a TMPyP–OTs solution after irradiation at 423 nm for various times. The inset shows the dependence of absorbance at the Soret band maximum on exposure time. (**b**) The 650 nm photoluminescence intensity for TMPyP–OTs (100 µL DMSO + 1 mL H_2O) under argon bubbling in logarithmic coordinates (black curve) and linear fit (red line).

Therefore, conclusions about the degradation rate constant for all porphyrins were based on fluorescence spectra in order to standardize the experimental conditions. Moreover, this method was chosen for further work because luminescence is more sensitive to low concentrations—even single molecules can contribute to the signal. The duration of each measurement was about 1 h. The dependence of photoluminescence on exposure time for TMPyP–OTs is presented in Figure 4b. The curve is plotted on a logarithmic scale to obtain linearizing coordinates for a first-order reaction. The obtained plots were approximated by a linear function. The linearity of the dependence confirms the assumed reaction order, and the slope of the straight line is the apparent reaction rate constant. Data on the degradation rate are presented in Table 1.

Under identical solvent conditions (100 µL DMSO + 1 mL H_2O) and aerobic atmosphere, the apparent rate constants increased in the order TPP (0.033 min^{-1}) < ZnTPP (0.046 min^{-1}) < TMPyP–OTs (0.139 min^{-1}), corresponding to decreasing photostability (Table 1). Argon deaeration reduced all rate constants, with the largest relative effect for TMPyP–OTs (Table 1), confirming the dominant contribution of oxygen-dependent pathways. The solvent effect was evaluated for TMPyP–OTs: DMSO accelerated degradation under air, while after oxygen removal the effect decreased (Table 1). With an increase in

temperature from 25 to 45 °C, the photodegradation rate constant of aqueous TMPyP–OTs under argon increased by a factor of 2.5 (Figure 5).

Table 1. Rate constants of porphyrin photodegradation.

Porphyrin	Solvent	Concentration, μM	k, min^{-1}	k, min^{-1} Argon Bubbling
TPP	100 μL DMSO + 1 mL H_2O	0.22 ± 0.01	0.033 ± 0.002	0.013 ± 0.001
ZnTPP	100 μL DMSO + 1 mL H_2O	0.17 ± 0.01	0.046 ± 0.003	0.028 ± 0.002
TMPyP–OTs	100 μL DMSO + 1 mL H_2O	0.45 ± 0.01	0.139 ± 0.001	0.034 ± 0.002
TMPyP–OTs	H_2O	0.45 ± 0.01	0.026 ± 0.002	0.021 ± 0.001

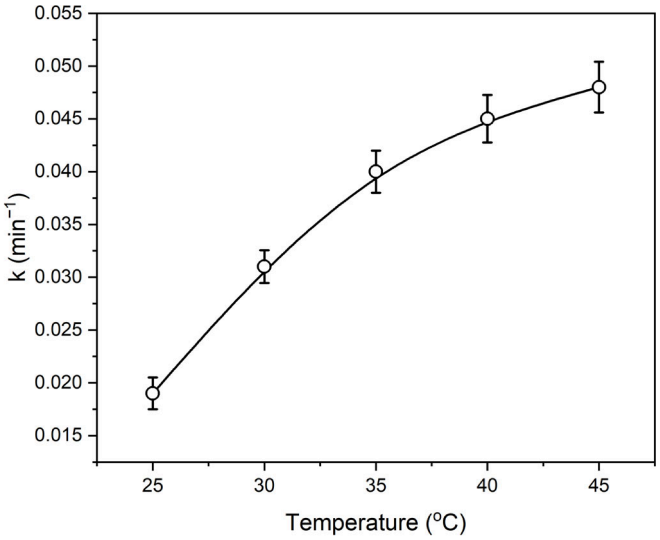


Figure 5. Effect of temperature on the photodegradation rate of aqueous TMPyP–OTs under argon bubbling.

4. Discussion

The ranking in Table 1 can be rationalized by the interplay of steric shielding, metalation, and aggregation. The low degradation rate of TPP is consistent with steric protection of the meso positions by phenyl groups, which hinders attack by reactive species, especially singlet oxygen. Although this shielding does not completely block degradation, it significantly slows the process.

The faster degradation of ZnTPP compared with TPP is attributed to heavy-atom-enhanced intersystem crossing. The presence of the Zn^{2+} ion in the center of the macrocycle accelerates intersystem crossing due to the heavy-atom effect, increasing the yield of the triplet state and, consequently, the generation of singlet oxygen [32]. As a result, the oxygen-dependent photooxidation pathway becomes more efficient, and the apparent photodegradation rate increases.

For TMPyP–OTs, the situation is more complex. However, its reduced photostability cannot be attributed to steric shielding, since the meso-substituents occupy the same positions as in TPP and are at least as bulky. Likewise, the explanation should not be reduced to a specific nitrogen site: the pyridinium nitrogens are quaternized and are not the primary oxidation centers, while the free-base character of TMPyP–OTs may contribute to its higher oxidation sensitivity relative to metallated ZnTPP but cannot account for its faster degradation than free-base TPP. A more consistent explanation is the aggregation behavior of TMPyP–OTs: as a cationic water-soluble porphyrin in a water-rich DMSO/water medium, it

is prone to aggregation, and aggregation can markedly modulate singlet oxygen generation and the local concentration of reactive species. In the present case, the pronounced acceleration of the degradation of TMPyP–OTs under air, together with the strong attenuation of this acceleration after argon deaeration, is consistent with an aggregation-dependent enhancement of the oxygen-mediated pathway, including an increased local concentration of singlet oxygen and, possibly, contributions from triplet–triplet annihilation. This interpretation also agrees with literature data showing that aggregation can either suppress or enhance $^1O_2$ production depending on the aggregation mode and environment [33].

The solvent effect provides further insight. The effect of DMSO is explained by the formation of DMSO–water clusters and a change in the microenvironment of the solvated molecules. Presumably, this occurs due to changes in solvation and a decrease in the viscosity of the medium, which can increase the singlet oxygen yield [34]. In the absence of oxygen, the influence of the organic solvent is weaker, although oxygen-independent electron-transfer pathways may still be affected.

Golec et al. [30] demonstrated for tetraphenylporphyrin and its zinc complex in toluene that deaeration increases the quantum yield of photodegradation while decreasing the measured rate of photobleaching, because oxygen removal simultaneously suppresses oxygen-dependent chemistry and extends the triplet lifetime from hundreds of nanoseconds to hundreds of microseconds. This highlights the need to distinguish apparent kinetic constants from intrinsic photodegradation efficiencies. In our experiments, argon bubbling reduced the apparent rate constants for all three porphyrins (Table 1), which identifies the oxygen-dependent pathway as dominant under air. This observation is fully consistent with Golec et al., because the suppression of the dominant channel outweighs the increased contribution of oxygen-independent pathways. The temperature dependence of TMPyP-OTs in deaerated water (a 2.5-fold increase from 25 to 45 °C) is likewise consistent with the picture of Golec et al.: once oxygen is removed, slower, thermally activated oxygen-independent channels become detectable. At the same time, the effect of DMSO in our system differs from that reported by Golec et al., who found that DMSO complexation can increase photostability. In our case, DMSO accelerated the degradation of TMPyP-OTs under air (5.3-fold) and much less after deaeration (1.6-fold). This difference indicates that the effect of DMSO is porphyrin-specific and depends on the mode of DMSO interaction (axial complexation versus solvation and viscosity change), and it cautions against treating DMSO as a universal stabilizer or quencher.

Lopes et al. [31] showed for meso-tetrapyridyl zinc(II) porphyrin that the fluorescence profile and intensity depend on the excitation wavelength and on solvent composition, and that methanol-induced quenching is mediated by hydrogen bonding to the pyridyl fragments, reflecting changes in the population of excited-state relaxation pathways. This result is directly relevant to our system, in which the pyridinium groups of TMPyP-OTs can engage in specific interactions with water and DMSO. Accordingly, the decrease in 650-nm luminescence intensity observed here should be regarded as a composite response that may include both chemical degradation and photophysical effects such as hydrogen-bond-mediated quenching or solvent-induced changes in excited-state relaxation. For this reason, the constants in Table 1 are reported and discussed as apparent constants characterizing the overall change in the luminescence response under the given conditions. The ranking of photostability (TPP > ZnTPP > TMPyP-OTs) and the conclusion that oxygen-dependent pathways dominate under air are directly supported by the experiments, whereas the attribution of the enhanced degradation of TMPyP-OTs to aggregation-dependent effects, including a possible contribution from triplet–triplet annihilation and an increased local concentration of singlet oxygen, is presented as a plausible interpretation consistent with the literature rather than as a direct experimental finding. A definitive separation of chemical

and photophysical contributions would require independent absorption measurements in the Soret band and, ideally, absolute measurements of photodegradation quantum yields, which we identify as a direction for future work.

The temperature dependence of TMPyP–OTs photodegradation in deaerated water provides further evidence for oxygen-independent pathways. Because the oxygen-dependent mechanism was suppressed by argon, this acceleration is likely due to faster electron transfer from the solvent to the excited porphyrin [35], faster protonation of porphyrin radical anions, and changes in viscosity and aggregation equilibrium [33]. These factors increase the probability of irreversible macrocycle transformation.

Overall, the results show that the photostability of porphyrins in hybrid molecular–plasmonic nanomaterials cannot be predicted from structure alone. Metalation, peripheral substituents, aggregation state, oxygen concentration, solvent composition, and temperature must be considered together. For photomedicine and bioimaging, these factors determine whether a porphyrin-based luminophore will retain its signal and therapeutic function during irradiation. In particular, TPP-like structures with steric protection may be preferable when high photostability is required, whereas the higher reactivity of TMPyP–OTs may be useful in PDT but its use requires careful control of oxygen and solvent conditions.

5. Conclusions

The photostability of TPP, ZnTPP, and TMPyP–OTs was quantified in water and DMSO/water mixtures, and the key structural and environmental factors controlling their photodegradation were identified. Under air in DMSO/water, photostability decreased in the order TPP > ZnTPP > TMPyP–OTs. The lowest stability of TMPyP–OTs is attributed to a combination of free-base character (relative to ZnTPP) and aggregation propensity, with aggregation providing the more consistent explanation for its faster degradation than TPP. Argon deaeration significantly slowed the degradation of all porphyrins, especially TMPyP–OTs, confirming the dominant role of oxygen-dependent pathways under air. DMSO accelerated degradation under aerobic conditions, while its effect weakened after oxygen removal, linking the solvent effect to singlet-oxygen-mediated processes. In deaerated water, the photodegradation of TMPyP–OTs was temperature-dependent, indicating a significant oxygen-independent contribution.

The rate constants reported here are apparent constants reflecting the overall change in the luminescence response under the specified conditions. The ranking of photostability and the dominant role of oxygen-dependent pathways are directly supported by the experimental data, whereas the mechanistic attribution to aggregation-dependent enhancement of singlet oxygen generation is an interpretation consistent with the literature. Separation of chemical degradation from photophysical quenching will require independent absorption-based kinetic measurements and absolute quantum yield determinations in future work. These findings provide selection criteria for porphyrin-based luminophores in hybrid nanomaterials: TPP-like scaffolds are preferable when high photostability is required, whereas the higher reactivity of TMPyP–OTs is advantageous for photodynamic therapy under carefully controlled oxygen and solvent conditions.

Author Contributions: Conceptualization, A.P. (Alexey Povolotskiy) and L.V.; methodology, L.V.; validation, L.V., E.C. and D.L.; formal analysis, L.V.; investigation, L.V.; data curation, E.C.; writing—original draft preparation, A.P. (Anastasia Povolotckaia); writing—review and editing, A.P. (Anastasia Povolotckaia); visualization, L.V. and D.L.; supervision, A.P. (Alexey Povolotskiy); project administration, A.P. (Alexey Povolotskiy). All authors have read and agreed to the published version of the manuscript.

Funding: This research was funded by Saint-Petersburg State University, project № 122040800256-8.

Institutional Review Board Statement: Not applicable.

Data Availability Statement: The data presented in this study are available on request from the corresponding author.

Acknowledgments: This study was performed at the Center for Optical and Laser Materials Research (Research Park, Saint-Petersburg State University).

Conflicts of Interest: The authors declare no conflicts of interest.

References

1. Zakavi, S.; Gharab, N.G. Interaction of para-substituted meso-tetraphenylporphyrins and meso-tetra(n-propyl)porphyrin with weak and strong carboxylic acids: A UV–Vis spectroscopic study. *Polyhedron* **2007**, *26*, 2425–2432. [CrossRef]
2. Zakavi, S.; Omidyan, R.; Ebrahimi, L.; Heidarizadi, F. Substitution effects on the UV–vis and 1H NMR spectra of the dications of meso and/or β substituted porphyrins with trifluoroacetic acid: Electron-deficient porphyrins compared to the electron-rich ones. *Inorg. Chem. Commun.* **2011**, *14*, 1827–1832. [CrossRef]
3. Rosa, A.; Ricciardi, G.; Baerends, E. Effects of porphyrin core saddling, meso-phenyl twisting, and counterions on the optical properties of meso-tetraphenylporphyrin diacids: The H4TPP2 (X = F, Cl, Br, I) Series as a Case Study. *J. Phys. Chem. A* **2003**, *107*, 11468–11482. [CrossRef]
4. Weinkauf, J.R.; Cooper, S.W.; Schweiger, A.; Wamser, C.C. Substituent and solvent effects on the hyperporphyrin spectra of diprotonated tetraphenylporphyrins. *J. Phys. Chem. A* **2003**, *107*, 3486–3496. [CrossRef]
5. Webb, M.J.; Bampos, N. Noncovalent interactions in acid–porphyrin complexes. *Chem. Sci.* **2012**, *3*, 2351–2366. [CrossRef]
6. Goldberg, P.K.; Pundsack, T.J.; Splan, K.E. Photophysical investigation of neutral and diprotonated free-base bis(arylethynyl)porphyrins. *J. Phys. Chem. A* **2011**, *115*, 10452–10460. [CrossRef] [PubMed]
7. Dyrda, G.; Słota, R.; Broda, M.A.; Mele, G. Meso-aryl-substituted free-base porphyrins: Formation, structure and photostability of diprotonated species. *Res. Chem. Intermed.* **2016**, *42*, 3789–3804. [CrossRef]
8. Cavaleiro, J.A.S.; Görner, H.; Lacerda, P.S.S.; MacDonald, J.G.; Mark, G.; Neves, M.G.P.M.S.; Nohr, R.S.; Schuchmann, H.P.; von Sonntag, C.; Tomé, A.C. Singlet oxygen formation and photostability of meso-tetraarylporphyrin derivatives and their copper complexes. *J. Photochem. Photobiol. A Chem.* **2001**, *144*, 131–140. [CrossRef]
9. Zakavi, S.; Hoseini, S.; Mojarrad, A.G. New insights into the influence of weak and strong acids on the oxidative stability and photocatalytic activity of porphyrins. *New J. Chem.* **2017**, *41*, 11053–11059. [CrossRef]
10. Sobbi, A.K.; Wöhrle, D.; Schlettwein, D. Photochemical stability of various porphyrins in solution and as thin film electrodes. *J. Chem. Soc. Perkin Trans.* **1993**, *2*, 481–488. [CrossRef]
11. Rotomskis, R.; Bagdonas, S.; Streckyte, G. Spectroscopic studies of photobleaching and photoproduct formation of porphyrins used in tumour therapy. *J. Photochem. Photobiol. B Biol.* **1996**, *33*, 61–67. [CrossRef] [PubMed]
12. Rotomskis, R.; Streckyte, G.; Bagdonas, S. Phototransformations of sensitizers—Significance of the nature of the sensitizer in the photobleaching process and photoproduct formation in aqueous solution. *J. Photochem. Photobiol. B Biol.* **1997**, *39*, 167–171. [CrossRef]
13. Melo, C.A.S.; Bagnato, V.S.; Imasato, H.; Perussi, J.R. Spectroscopic studies of photobleaching and photoproduct of the photosensitizer Photogem during intense illumination. *Laser Phys.* **2004**, *14*, 1214–1218.
14. Menezes, P.F.C.; Imasato, H.; Bagnato, V.S.; Sibata, C.H.; Perussi, J.R. Influence of pH on the phototransformation process of Photogem®. *Laser Phys.* **2009**, *19*, 1457–1462. [CrossRef]
15. Mathai, S.; Smith, T.A.; Ghiggino, K.P. Singlet oxygen quantum yields of potential porphyrin-based photosensitisers for photodynamic therapy. *Photochem. Photobiol. Sci.* **2007**, *6*, 995–1002. [CrossRef] [PubMed]
16. Lassalle, H.P.; Bezdetnaya, L.; Iani, V.; Juzeniene, A.; Guillemin, F.; Moan, J. Photodegradation and phototransformation of 5,10,15,20-tetrakis(m-hydroxyphenyl)bacteriochlorin (m-THPBC) in solution. *Photochem. Photobiol. Sci.* **2004**, *3*, 999–1005. [CrossRef] [PubMed]
17. Bonnett, R.; Martinez, G. Photobleaching of sensitisers used in photodynamic therapy. *Tetrahedron* **2001**, *57*, 9513–9547. [CrossRef]
18. Hadjur, C.; Lange, N.; Rebstein, J.; Monnier, P.; Bergh, H.; Wagnières, G. Spectroscopic studies of photobleaching and photoproduct formation of meta(tetrahydroxyphenyl)chlorin (m-THPC) used in photodynamic therapy. The production of singlet oxygen by m-THPC. *J. Photochem. Photobiol. B Biol.* **1998**, *45*, 170–178. [CrossRef]
19. Ericson, M.B.; Grapengiesser, S.; Gudmundson, F.; Wennberg, A.M.; Larko, O.; Moan, J.; Rosén, A. A spectroscopic study of the photobleaching of protoporphyrin IX in solution. *Lasers Med. Sci.* **2003**, *18*, 56–62. [CrossRef] [PubMed]
20. Cox, G.S.; Whitten, D.G. Mechanisms for the photooxidation of protoporphyrin IX in solution. *J. Am. Chem. Soc.* **1982**, *104*, 516–521. [CrossRef]

21. Moan, J.; Western, A.; Rimington, C. NATO ASI Series. In *Photosensitisation*; Moreno, G., Ed.; Springer: Berlin/Heidelberg, Germany, 1988; Volume H15, pp. 407–417.
22. Smith, K.M.; Brown, S.B.; Troxler, R.F.; Lai, J.J. Photooxygenation of meso-tetraphenylporphyrin metal complexes. *Photochem. Photobiol.* **1982**, *36*, 147–152. [CrossRef] [PubMed]
23. Matsuura, T.; Inoue, K.; Ranade, A.C.; Saito, I. Photooxygenation of magnesium meso-tetraphenylporphyrin. *Photochem. Photobiol.* **1980**, *31*, 23–26. [CrossRef]
24. Smith, K.M.; Brown, S.B.; Troxler, R.F.; Lai, J.J. Mechanism of photo-oxygenation of meso-tetraphenylporphyrin metal complexes. *Tetrahedron Lett.* **1980**, *21*, 2763–2766. [CrossRef]
25. Cavaleiro, J.A.S.; Hewlins, M.J.E.; Jackson, A.H.; Neves, M.G.P.M.S. Structures of the ring-opened oxidation products from meso-tetraphenylporphyrin. *J. Chem. Soc. Chem. Commun.* **1986**, *22*, 142–144. [CrossRef]
26. Cavaleiro, J.A.S.; Neves, M.G.P.M.S. The photo-oxidation of meso-tetraphenylporphyrins. *J. Chem. Soc. Perkin Trans.* **1990**, *1*, 1937–1943. [CrossRef]
27. Silva, A.M.S.; Neves, M.G.P.M.S.; Martins, R.R.L.; Cavaleiro, J.A.S.; Boschi, T.; Tagliatesta, P. Photo-oxygenation of meso-tetraphenylporphyrin derivatives: The influence of the substitution pattern and characterization of the reaction products. *J. Porphyr. Phthalocyanines* **1998**, *2*, 45–51. [CrossRef]
28. Bonnett, R.; Martinez, G. Photobleaching of compounds of the 5,10,15,20-tetrakis(m-hydroxyphenyl)porphyrin series (m-THPP, m-THPC, and m-THPBC). *Org. Lett.* **2002**, *4*, 2013–2016. [CrossRef] [PubMed]
29. Kruk, M.M.; Starukhin, A.S.; Maes, W. Influence of macrocycle protonation on the photophysical properties of porphyrins. *Macroheterocycles* **2011**, *4*, 69–79. [CrossRef]
30. Golec, B.; Buczyńska, J.; Nawara, K.; Gorski, A.; Waluk, J. Photodegradation of free base and zinc porphyrins in the presence and absence of oxygen. *Photochem. Photobiol. Sci.* **2023**, *22*, 2725–2734. [CrossRef] [PubMed]
31. Lopes, J.M.S.; Sampaio, R.N.; Dinelli, L.R.; Batista, A.A.; Araujo, P.T.; Barbosa Neto, N.M. On the excitation dependence of fluorescence spectra of meso-tetrapyridyl zinc(II) porphyrin and its relation with hydrogen bonding and outlying decoration. *Spectrochim. Acta Part A Mol. Biomol. Spectrosc.* **2020**, *224*, 117371. [CrossRef] [PubMed]
32. Tang, M.J.; Arriaga Gomez, J.C.; Manriquez, D.; Yao, X.; Hao, Y.; Chen, H.; Li, Y.; An, L.; Qi, L.; Farha, O.K.; et al. Photooxidation of Organic Sulfide Enhanced by Heavy Atom Effect in Porphyrin Metal–Organic Frameworks with a Sea Topology. *ACS Catal.* **2026**, *16*, 5004–5013. [CrossRef]
33. Zhuang, Z.; Li, J.; Shen, P.; Zhao, Z.; Tang, B.Z. Exploring and leveraging aggregation effects on reactive oxygen species generation in photodynamic therapy. *Aggregate* **2024**, *5*, e540. [CrossRef]
34. Nastasa, V.; Pascu, A.; Boni, M.; Smarandache, A.; Staicu, A.; Pascu, M.L. Insights into the photophysics of zinc phthalocyanine and photogenerated singlet oxygen in DMSO-water mixture. *Colloids Surf. A Physicochem. Eng. Asp.* **2016**, *505*, 197–203. [CrossRef]
35. Nakanishi, T.; Ohkubo, K.; Kojima, T.; Fukuzumi, S. Reorganization energies of diprotonated and saddle-distorted porphyrins in photoinduced electron-transfer reduction controlled by conformational distortion. *J. Am. Chem. Soc.* **2009**, *131*, 577–584. [CrossRef] [PubMed]

Disclaimer/Publisher's Note: The statements, opinions and data contained in all publications are solely those of the individual author(s) and contributor(s) and not of MDPI and/or the editor(s). MDPI and/or the editor(s) disclaim responsibility for any injury to people or property resulting from any ideas, methods, instructions or products referred to in the content.